

# *In situ* study of nanotemplate-induced growth of lysozyme microcrystals by submicrometer GISAXS

Eugenia Pechkova<sup>a</sup> and Claudio Nicolini<sup>b\*</sup>

Received 30 July 2009

Accepted 24 December 2010

<sup>a</sup>Nanoworld Institute, University of Genoa, Corso Europa 30, 16132 Genoa, Italy, and <sup>b</sup>Fondazione ELBA, Piazza SS Apostoli 66, 00187 Rome, Italy. E-mail: manuscript@ibf.unige.it

Ultrasmall lysozyme microcrystals are grown by classical hanging-drop vapor diffusion and by its modification using a homologous protein thin-film template displaying long-range order. The nucleation and growth mechanisms of lysozyme microcrystals are studied at the thin lysozyme film surface using a new *in situ*  $\mu$ GISAXS (microbeam grazing-incidence small-angle X-ray scattering) technique recently developed at the microfocus beamline of the ESRF in Grenoble, France. New insight on the nucleation and crystallization processes appear to emerge.

© 2011 International Union of Crystallography  
Printed in Singapore – all rights reserved**Keywords:** GISAXS; microbeam; protein crystallization.

## 1. Introduction

Techniques of elastic scattering of X-rays are widely used as they provide valuable tools for probing the order properties of protein crystals. By careful analysis of the integrated diffracted intensities one can access the atomic structure, *i.e.* the positions of nuclei and the spread of the electronic cloud around atoms. Small-angle X-ray scattering (SAXS) involves instead techniques which allow information to be obtained at scales that are greater than the interatomic distances. In ordered materials this domain is restricted in between the first Bragg peak which overlaps with the direct beam and the diffraction peaks (Guinier & Fournet, 1955; Guinier, 1963). The growth of the field of thin films has led to studies on layer morphology and on sizes of quantum dots, supported islands or buried particles, which has pushed down the size of the incoming beam to the micrometer level (Gehrke, 1992). The development of microbeam grazing-incidence SAXS ( $\mu$ GISAXS) (Müller-Buschbaum *et al.*, 2000, 2003; Roth *et al.*, 2003; Renaud *et al.*, 2009) has provided information at the highest sensitivity down to the nanometer scale on the dependence of electronic density perpendicular to surfaces, *e.g.* the roughness of a surface, lateral correlations, and the size and shape of gold nanoparticles (Roth *et al.*, 2003).

$\mu$ GISAXS as an advanced scattering method permits investigation of large-scale structures in thin films (Rauscher *et al.*, 1995; Müller-Buschbaum *et al.*, 2003). First protein nanotemplate crystallization experiments were successfully established *ex situ* (Pechkova *et al.*, 2005; Nicolini & Pechkova, 2004) and here are now carried out *in situ* in order to overcome the partial limitations of *ex situ* discontinuous experiments with lysozyme (Pechkova & Nicolini, 2006) and P450<sub>scc</sub> cytochrome (Nicolini & Pechkova, 2006). Such information is of prime interest in understanding the link between growing ultrasmall lysozyme crystal morphology and its physical,

chemical and structural properties, the latter being also the object of work down to atomic resolution by X-ray microfocus diffraction (Riekkel, 2000; Pechkova & Nicolini, 2010) and of the recent *in situ* GISAX layout (Pechkova *et al.*, 2010a) and experimentation on thaumatococcus (Gebhardt *et al.*, 2010).

Moreover, this method seems to produce more radiation-stable crystals than those obtained by classical techniques (Pechkova *et al.*, 2004, 2009, 2010b). This aspect also concerns crystals of miniscule thickness (5–20  $\mu$ m) such as the human kinase crystal used for its three-dimensional structure determination by diffraction using synchrotron microfocus beam (Pechkova *et al.*, 2003).

## 2. Materials and methods

Lysozyme monolayers were deposited on glass slides by the Langmuir–Schaefer method (Nicolini, 1997; Pechkova & Nicolini, 2004a).

### 2.1. Homologous nanobiofilm template

An innovative crystallization method is described by Pechkova & Nicolini (2002a,b). A protein thin-film nanotemplate is created using Langmuir–Blodgett (LB) technology or modifications of it, *i.e.* Langmuir–Schaeffer (LS), and is subsequently deposited on a solid glass support (cover slide) and dried in nitrogen flux. The droplet of protein/precipitant solution has to be placed over the protein nanofilm on the glass slide and then introduced to the appropriate vapor-diffusion crystallization cell, as in the traditional hanging-drop vapor-diffusion method. This LS lysozyme nanofilm assumes the role of the template for lysozyme nucleation and crystal growth. The lysozyme crystallization conditions for the protein nanofilm crystallization method were the same as for the traditional hanging-drop vapor-diffusion method (see

below). Further details of the parameters of the lysozyme microcrystal growth are provided by Pechkova *et al.* (2009, 2010*b*) and Pechkova & Nicolini (2002*a,b*).

### 2.2. Flow-through crystallization cell

The flow-through crystallization cell was designed in order to perform *in situ* GISAX measurements during protein nucleation and crystal growth in real time. A hanging-drop set-up was used for the lysozyme crystallization: the droplet, containing 20 mg ml<sup>-1</sup> lysozyme in 50 mM sodium acetate buffer (pH 4.5) and 0.45 M NaCl, was placed onto a glass circle cover slide of diameter 12 mm, which was glued onto the inner cylinder of the flow-through crystallization cell (classical method). In the case of nanotemplate crystallization the glass cover slide was previously covered with LS lysozyme nanofilm (Fig. 1). Two kapton windows were inserted into the outer cell walls to perform a scattering experiment under grazing-incidence conditions. For rapid buffer exchange the reservoir was connected *via* Teflon tubes to two Harvard syringe pumps. An equation for determining the buffer concentration  $c_G$  as a function of time was derived for this special set-up (Pechkova *et al.*, 2010*b*),

$$c_G(t) = \frac{c_0(t_0)V_0 + c_1(dV_1/dt)dt}{V_0 + (dV_{12}/dt)dt} \quad (1)$$

The initial concentration of the reservoir at  $t = 0$  with volume  $V_0$  is given by  $c_0$ ;  $dV_1/dt$  denotes the incoming flux with concentration  $c_1$ . The outgoing flux is given by  $dV_{12}/dt$ . During the beam alignment the NaCl concentration in the reservoir

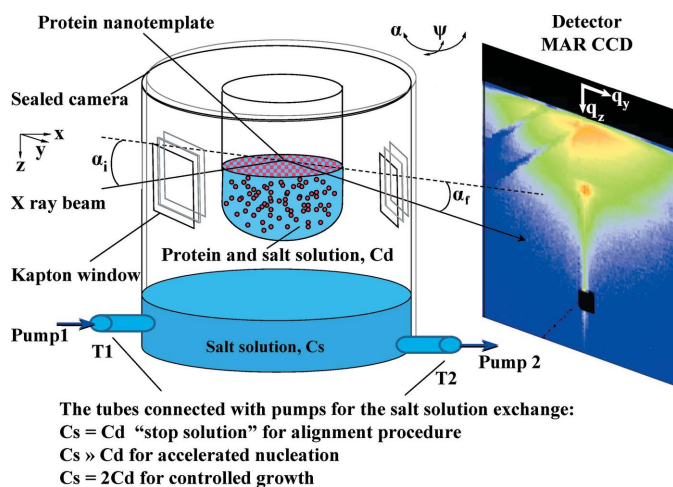


**Figure 1** Schematic view of the *in situ*  $\mu$ GISAXS set-up at ID13/ESRF. The experimental layout of the vapor deposition cylinder is also shown, containing two stainless windows transparent to the X-rays and the lysozyme solution typical droplet hanging on the lysozyme two layers deposited over the glass. The cylinder is mounted on an  $xyz$  gantry and a two-axis goniometer ( $\phi_x, \phi_y$ ). The scan is made in the  $y$  direction.  $\alpha_i$  denotes the angle between the incident beam and the sample surface,  $\alpha_f$  the corresponding exit angle, and  $2\phi$  the out-of-plane angle. The flight path ( $L = 1.15$  m) between the sample and the two-dimensional detector is evacuated ( $10^{-2}$  mbar). On the right is shown the typical two-dimensional  $\mu$ GISAXS signal of the lysozyme drop sitting on a layer.

solution was kept equal to that in the droplet, 0.45 M (stop solution). The experiment, described in detail by Pechkova *et al.* (2010*a*), consists of two parts: accelerated nucleation for 20 min (four-times-higher NaCl concentration in the reservoir with respect to the drop, *i.e.* 1.8 M), and controlled growth up to 24 h (two-times-higher salt concentration, *i.e.* 0.9 M).

Crystallization experiments were carried out for  $\mu$ GISAXS study with and without the nanotemplate under the conditions described in detail by Pechkova & Nicolini (2006) and Pechkova *et al.* (2010*a*).

We performed a preliminary lysozyme crystallization experiment using the classical hanging-drop method under accelerated-nucleation conditions for the first 20 min and under controlled-growth conditions for 22 h thereafter. Under these conditions about 12 lysozyme crystals with an average crystal size of  $\sim 20 \mu\text{m}$  were observed after 16 h. At the end of this preliminary experiment it was found that a drop of the original 6  $\mu\text{l}$  volume contained about 60 crystals of average crystal size  $\sim 75\text{--}105 \mu\text{m}$ . The experiment was highly successful since it proved that under the conditions hypothesized earlier we can actually perform controlled nucleation and growth of the lysozyme crystal within 10 h.

During the  $\mu$ GISAXS study, two (classical and LB) parallel experiments were conducted on the bench under the same conditions. Using the LB nanotemplate method the first 10  $\mu\text{m}$  crystal was visible by light microscopy at  $6\times$  magnification at 1.5 h after plating; 300 crystals of size 15–20  $\mu\text{m}$  were visible at 2.5 h and progressive growth resulted in more than 1000 crystals of size 70–80  $\mu\text{m}$ , with ten crystals above 90  $\mu\text{m}$  and a complete filling of the entire drop at 21.5 h after plating. For the classical crystallization experiment no crystals were visible at  $6\times$  magnification up to 14 h when 20 crystals of about 25  $\mu\text{m}$  appeared. Then, two crystals of 120  $\mu\text{m}$  and more than 100 crystals of 30  $\mu\text{m}$  were visible after 19.5 h. At the end of the experimental observation (21.5 h after plating) there were over 150 crystals of  $\sim 90 \mu\text{m}$  with two crystals of 150  $\mu\text{m}$  in the droplet (Pechkova *et al.*, 2010*a*).

During the real-time  $\mu$ GISAXS study of the lysozyme sample in the crystallization flow-through cell in the presence of LB film the data were acquired for 1 s at a time interval of 2 min in the first 30 min, and at  $t = 26$  min the acquisition time was changed to 5 s and the signal increased. Images were recorded up to a total of 93, periodically translating the direction of the incoming beamline in the experiment by 10  $\mu\text{m}$ .

In the classical hanging-drop *in situ*  $\mu$ GISAXS experiment data were acquired for 5 + 5 s at a time interval of 110 s from 30 min up to 3 h; a total of 268 images were recorded in the 9 h 36 min period after the beginning of the experiment.

After 22 h of experiments on the beamline we monitored the crystals that had grown in the flow-through crystallization cell both under the classical hanging-drop conditions and in the presence of the LB nanotemplate. The 6  $\mu\text{l}$  drop was completely filled with crystals of  $\sim 100\text{--}120 \mu\text{m}$  in the case of the LB method while in the classical hanging-drop method about 150 crystals of length  $\sim 80\text{--}90 \mu\text{m}$  were observed.

### 2.3. Microbeam-GISAXS experiments using synchrotron radiation

Microbeam-GISAXS as an advanced scattering method permits investigation of large-scale structures in thin films (Rauscher *et al.*, 1995; Müller-Buschbaum *et al.*, 2003). First *ex situ* protein nanotemplate crystallization experiments were successfully established (Pechkova *et al.*, 2005). Micro-GISAXS experiments were performed at the ID13 microfocus beamline (Riekkel, 2000) at the European Synchrotron Radiation Facility in Grenoble, France. The incoming monochromatic beam ( $\lambda = 0.991 \text{ \AA}$ ,  $E = 12519 \text{ eV}$ ) was focused using a set of two Fresnel lenses. The size of the beam in grazing-incidence geometry is given by  $S = X_v/\tan(\alpha_i)$ , where  $\alpha_i$  is the angle of incidence of the beam on the sample and  $X_v$  is the vertical beam size. For a typical angle  $\alpha_i = 0.71^\circ$  (see Fig. 1) and  $X_v = 1 \text{ }\mu\text{m}$  one calculates  $S = 87 \text{ }\mu\text{m}$ . The  $0.5 \text{ }\mu\text{m} \times 1 \text{ }\mu\text{m}$  beam size (full width at half-maximum, vertical  $\times$  horizontal) at the focal spot position on the sample surface is elongated in the beam direction. A micro-ionization chamber with a  $20 \text{ }\mu\text{m}$  guard aperture was used to monitor the beam intensity and to reduce parasitic scattering. The flux on the sample was around  $10^{10} \text{ photons s}^{-1}$ . The direct beam was blocked by a  $300 \text{ }\mu\text{m}$ -diameter beamstop to avoid over-exposure of the detector. A temporal intensity variation is observed in the angular range from  $0.1^\circ$  to  $0.4^\circ$ .

The flow-through crystallization cell of Fig. 1 was placed on a two-axis goniometer with rotating angle ( $\alpha$ ,  $\psi$ ), mounted on an  $x/y/z$  translation unit with the X-ray beam direction along the  $x$ -axis (Fig. 1). The crystallization cell was tilted by the goniometer to adjust the fixed angle of incidence ( $\alpha_i = X^\circ$ ). The  $\mu$ GISAXS patterns were recorded using a MAR165 CCD detector ( $78.94 \text{ }\mu\text{m} \times 78.94 \text{ }\mu\text{m}$  pixel size;  $2 \text{ K} \times 2 \text{ K}$  pixels; 16-bit readout). The sample-to-detector distance was  $791 \text{ mm}$ , determined by a Ag-behenate standard (Blanton *et al.*, 1995).

Based on the coordinate system of the sample in the  $x$ - $y$  plane the incoming beam is directed along the  $x$ -axis and impinges on the sample at an incident angle  $\alpha_i$ . The beam is specularly ( $q_x = q_y = 0$ ,  $q_z > 0$ ) and diffusely ( $q_x, q_y \neq 0$ ) scattered;  $q' = (q_x, q_y, q_z)$  denotes the scattering vector. The intensity signal was recorded using a MAR165 CCD detector ( $78.94 \text{ }\mu\text{m} \times 78.94 \text{ }\mu\text{m}$  pixel size;  $2 \text{ K} \times 2 \text{ K}$  pixels; 16-bit readout). Along  $q_z$  at  $q_y = 0$  correlations vertical to the sample surface can be probed. The specular and the so-called Yoneda peak occur as a characteristic pattern. The specular peak appears if the specular condition ( $\alpha_i = \alpha_f$ ) is fulfilled. The so-called Yoneda peak (Yoneda, 1963) occurs at the critical angle of the sample,  $\alpha_f = \alpha_c$ . In the out-of-plane area of the two-dimensional GISAXS signal ( $q_y \neq 0$ ) diffusely scattered intensity is observed. Characteristic morphological parameters such as shape and distances of the sample can be extracted by analysis of out-of-plane scans in the  $q_y$  direction. The layout of the scattering measurements using the reference Cartesian frame has its origin on the surface and is defined by its  $z$ -axis pointing upwards, its  $x$ -axis perpendicular to the detector plane and its  $y$ -axis along the detector plane (Fig. 1). The light is scattered by any type of roughness on the surface.

Owing to energy conservation the scattering wavevector  $\mathbf{q}$  is the central quantity to be monitored during the measurements. As shown by Roth *et al.* (2003) the  $q_y$ -dependence (out-of-plane scans) reflects the structure and morphology parallel to the sample surface plane (distances  $D$ , in-plane radius  $R$ ) while the  $q_z$ -dependence (detector scans) reflects the height  $H$  of clusters, or the roughness parallel to the sample surface, with

$$q_y = 2\pi/\lambda \sin(2\theta) \cos(\alpha_f),$$

$$q_z = 2\pi/\lambda \sin(\alpha_i + \alpha_f).$$

As shown in Fig. 1 the scattering intensity is recorded on a plane ensuring that the angles are in the range of a few degrees, thus enabling study of lateral sizes of a few nanometers.

For data reduction and analysis the *Fit2D* software package was used and further data processing is planned to quantitatively probe the surface and interface morphology with *ab initio* considerations (Renaud *et al.*, 2009).

### 3. Results

The  $\mu$ GISAXS data are acquired during the nucleation and crystallization steps of lysozyme at various time intervals as described in §2, namely 93 frames over 22 h for LB data and 263 data frames over 21.5 h for classical data. The two-dimensional scattering patterns (Fig. 1) of  $q_z$  (detector scan) versus  $q_y$  (out-of-plane scan), being a function of morphological features at the surface and at the interface, appear to vary significantly for the lysozyme grown either by the nanotemplate-assisted method or by the classical vapor diffusion. As typical features the Yoneda peak at  $\alpha_c$  and the specular peak at  $\alpha_f = \alpha_i$  are shown in the two-dimensional GISAXS patterns, shown at the start and the end images, respectively, of lysozyme crystallization without (Fig. 2) and with (Fig. 3) the homologous nanotemplate. A subsequent quantitative analysis is in progress from the software being developed by Lazzari to quantitatively evaluate features such as microcrystal cluster diameters, heights and distances (Lazzari, 2002).

Comparison of Fig. 4 with Fig. 5 shows the clear effect on nucleation and growth of the lysozyme microcrystals, possibly due also to the microcrystals being clearly formed in the drop as a result of the presence of the homologous LB nanotemplate. Interestingly, while the two peaks in the Yoneda region appear to be already present at the start of plating with the LB nanotemplate (Fig. 4), without the LB nanotemplate they are absent at the start and present only at the end (Fig. 5). The changes in detector cut  $q_z$  appear to increase dramatically in magnitude with increasing acquisition time for the LB sample upon each periodic  $10 \text{ }\mu\text{m}$  translation of the direction of the incoming beamline (Fig. 6), while the similar modulation of the detector cut in the classical lysozyme growth appears quite less pronounced (Fig. 7). The lower peak in the overall diffuse scattering region is likely to correspond to the solution scattering (Nicolini & Pechkova, 2006) and appears to drastically

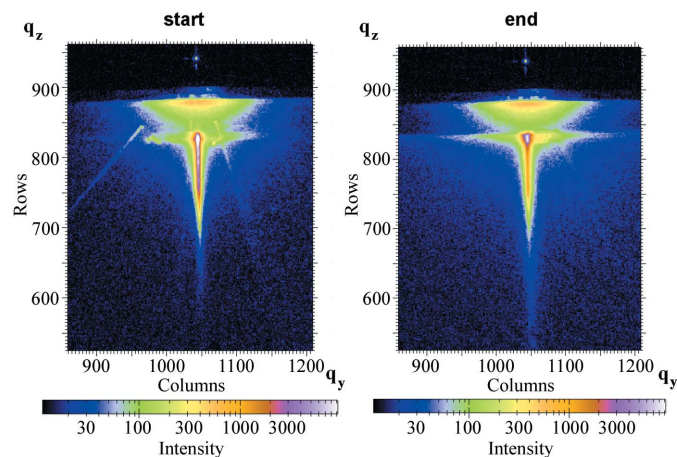


**Figure 2** Raw two-dimensional  $\mu$ GISAXS patterns of a classical lysozyme crystallizing hanging drop at 0 h after plating (start) and at the end of the experimental acquisition (end). Images were recorded as described in §2. Total  $\mu$ GISAXS patterns of  $q_y$  versus  $q_z$  in  $\text{\AA}^{-1}$  units are shown, where, owing to its high intensity, the specular peak is covered by a beamstop (in the upper part).

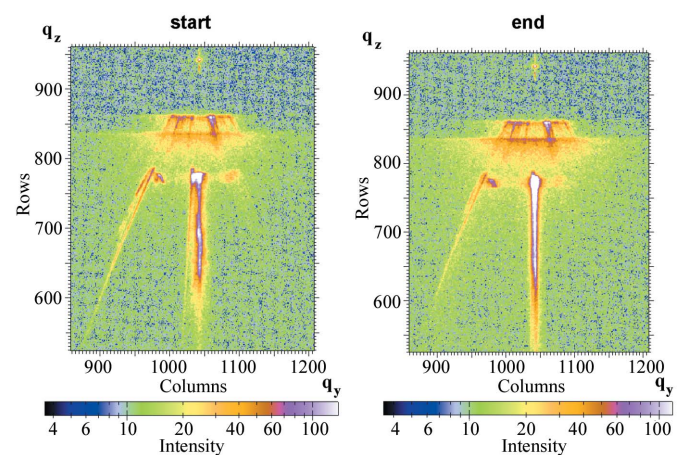


**Figure 3** Raw two-dimensional  $\mu$ GISAXS patterns of a lysozyme crystallizing hanging drop sitting over one monolayer of homologous lysozyme at 0 h after plating (start) and at the end of the experimental acquisition (end), using the nanotemplate-assisted hanging vapor diffusion method. Images were recorded as described in §2. Total  $\mu$ GISAXS patterns of  $q_y$  versus  $q_z$  in  $\text{\AA}^{-1}$  units are shown, where, owing to its high intensity, the specular peak is covered by a beamstop (in the upper part).

decrease in the classical crystal growth (Figs. 2 and 7) with respect to the LB nanotemplate growth (Figs. 3 and 6).

For this reason, in order to compare the crystallization process taking place with time in the presence and absence of protein film as nanotemplate, we have kept constant all conditions and obtained the following conclusions:

(i) The overall  $\mu$ GISAXS pattern of the drop containing lysozyme crystallizing solution based on the nanotemplate at all times after plating is constantly more pronounced with respect to the corresponding classical one; Fig. 2 shows two almost identical overall GISAXS patterns of the Yoneda peak, while only the Yoneda regions shown in Fig. 5 make it clear that the lower part of the pattern corresponds to glass scat-

tering while the upper part is protein scattering. The essential information for understanding the process is only apparent in Fig. 6 with the oscillation in intensity for the LB lysozyme crystals nucleation and growth.

(ii) In the Yoneda region of the corresponding  $\mu$ GISAXS pattern, being the most sensitive to structural and morphological changes of the surfaces owing to the interference effect involved in the occurrence of the Yoneda peak, contrary to the classical drops the nanotemplate-based lysozyme drops recorded at all times after plating clearly and constantly show at least two pronounced Yoneda peaks growing with time after plating, and after each translation of the incoming beam to overcome the crystal damage owing to the high radiation intensity under our experimental acquisition, similar to that shown in quantitative detail by *in situ* GISAXS for thaumatine crystals (Pechkova *et al.*, 2010a).

In the classical sample only a weak Yoneda peak exists at the start, with critical angle  $\alpha_f$  values corresponding to that of the glass substrate, while for the LB nanotemplate sample a second peak is also present at the start.

Hence all data are compatible with a working hypothesis which attributes the peak at higher  $\alpha_f$  values to that of the glass substrate, with the peak at lower  $\alpha_f$  values being related to the protein itself, either in the LB film or in the crystal.

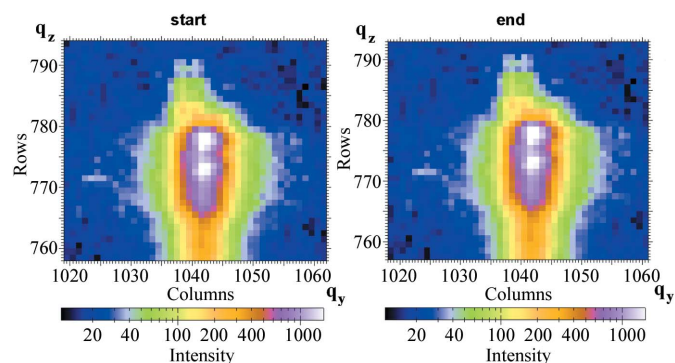


**Figure 4** Yoneda regions of the lysozyme nanotemplate-based drop. The patterns are shown on a logarithmic scale to enhance the features in the Yoneda regions.

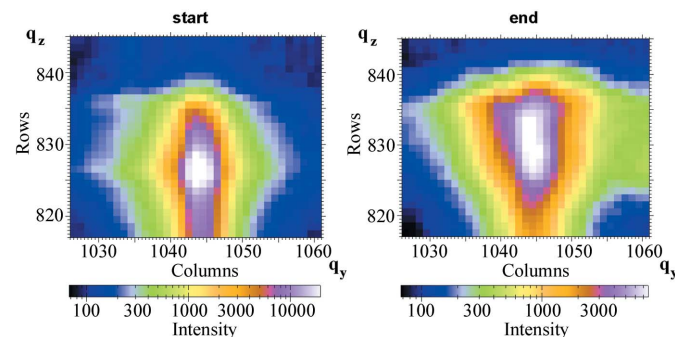


**Figure 5** Yoneda regions of the classical lysozyme drop. The patterns are shown on a logarithmic scale to enhance the features in the Yoneda regions. The Yoneda region represents the  $\alpha_f$  dependency at  $\alpha_i = 0.92$  of a classical lysozyme crystallizing drop at the start (left panel) and at the end (right panel).

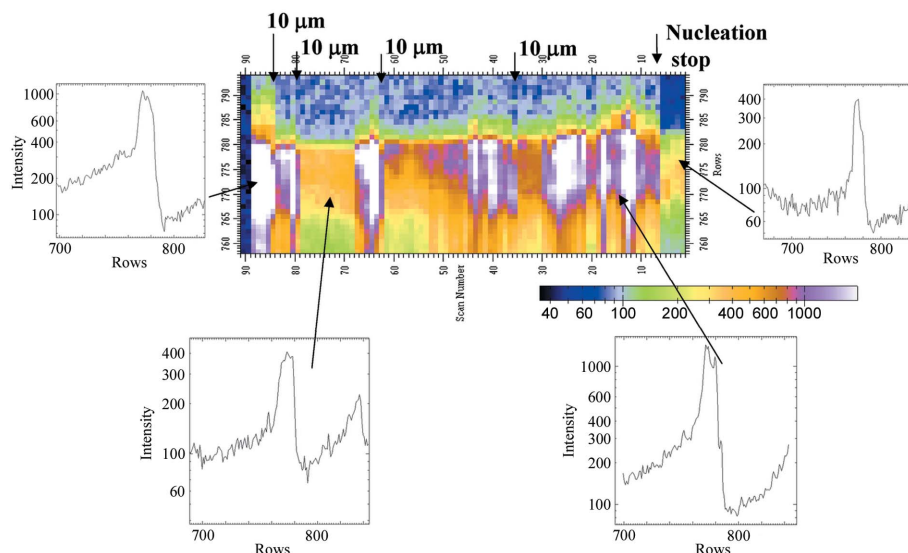


**Figure 6** Detector scans of the lysozyme LB nanotemplate drop *versus* time after plating (increasing frame number) over all the  $\mu$ GISAXS experiments described in §2. The panels show the projections along the center column of the detector scan with respect to the total  $\mu$ GISAXS scattering and the Yoneda regions.

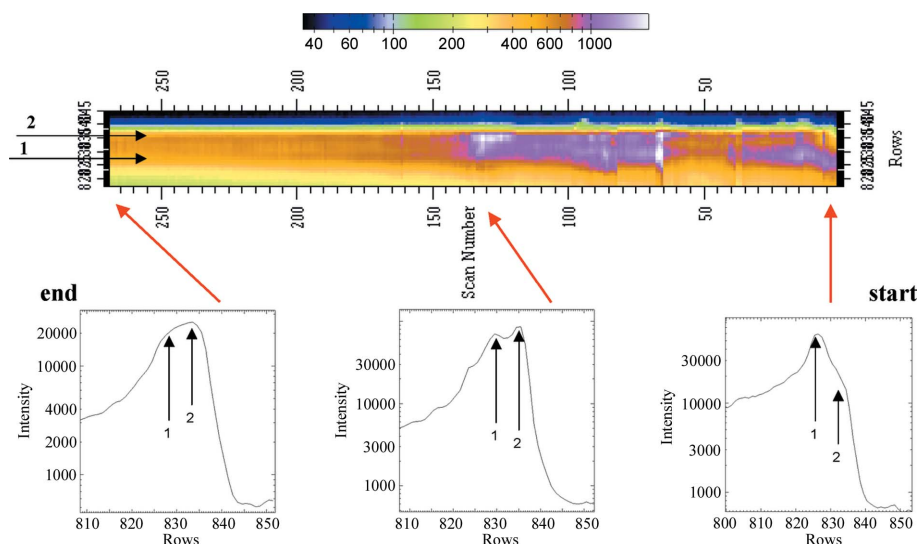


**Figure 7** Detector scans of the classical lysozyme drop *versus* time after plating (increasing frame number) over all the  $\mu$ GISAXS experiments described in §2. The panels show the projections along the center column of the detector scan with respect to the total  $\mu$ GISAXS scattering and the Yoneda regions.

#### 4. Conclusions

In summary, the data on LB intensity fluctuations in the GISAXS pattern *versus* time appear to be associated with rapid seed formation and crystal growth and damage, while the classic continuous shift of intensity in the Yoneda region is compatible with slow crystal growth and significantly larger damage, apparent by light microscopy both in the hatch and in the parallel experimentation carried out on the bench, quite compatible with the radiation damage being assessed by LB crystal diffractions (Pechkova *et al.*, 2009; radiation damage BAG experiments at ESRF) and that quantitatively reported

recently on the parallel crystallization experiment on thaumatin (Gebhardt *et al.*, 2010) using the same innovative submicrometer GISAXS layout described by Pechkova *et al.* (2010a). Streak appearance in the two-dimensional  $\mu$ GISAXS of Figs. 2 and 3 may be due to reflection on tilted crystal surfaces.

The kinetics and the structure of the growth of lysozyme microcrystals investigated here by *in situ*  $\mu$ GISAXS points to the superiority of the nanobiofilm template method (Pechkova & Nicolini 2004a,b) in inducing nucleation and growth, confirming earlier *ex situ*  $\mu$ GISAXS findings on the same lysozyme and on P450scc (Pechkova *et al.*, 2005; Pechkova & Nicolini, 2006; Nicolini & Pechkova, 2006), and very recent *in situ*  $\mu$ GISAXS on thaumatin (Pechkova *et al.*, 2010a; Gebhardt *et al.*, 2010). This approach with  $\mu$ GISAXS combines the powerful thin-film characterization method with the micrometer-sized X-ray beam enhancing the spatial resolution used thus far by two orders of magnitude (Pechkova *et al.*, 2004; Roth *et al.*, 2003). The acquired scattering data allow for a non-destructive and contact-free reconstruction of the nucleation and crystallization process at the very early stage. Such characterization and investigation on a submicrometer scale of extra-small crystal clusters on top of the protein film appears to allow a clearer understanding of the very early steps of lysozyme crystallization, similar to that being reported and explained using an analytical model fitting the thaumatin GISAXS data (Gebhardt *et al.*, 2010). It is worth noting that, even if the early *ex situ* data were quite illuminating (Pechkova *et al.*, 2004; Roth *et al.*, 2003),

more conclusive data have been obtained with the *in situ* experiments reported here and in the parallel papers (Gebhardt *et al.*, 2010; Pechkova *et al.*, 2010a). The older paper of Yoneda (1963) and the recent one by Renaud *et al.* (2009) have been frequently cited and, along with the models introduced by Nicolini & Pechkova (2006) and by Gebhardt *et al.* (2010), have been utilized to reach a conservative conclusion based on surface roughness and the analytical interpretation of the diffuse scattering. It is important to note that the set-up of beamline alignment with both vertical and horizontal scanning to locate the center of the drop was initially quite complicated and lengthy with this lysozyme experiment

contrary to the parallel experiment with thaumatin yielding a quantitative model capable of explaining the GISAXS observations (Gebhardt *et al.*, 2010).

This work is supported by FIRB-MIUR grant to the Biophysics Chair of the University of Genoa Medical School for Organic and Biological Nanosensors (RBPR05JH2P) and by a yearly MIUR grant to the Fondazione ElBA Nicolini for 'Funzionamento' (DM48527). We are grateful to the cooperation of Christian Riekkel, Ronald Gebhardt and Manfred Burghammer of ESRF and of Shailesh Tripathi of NWI in acquiring the  $\mu$ GISAXS data at ESRF. Recent significant experimentation is in progress under the radiation damage BAG umbrella at ESRF.

### References

- Blanton, T. N., Huang, T. C., Toraya, H., Hubbard, C. R., Robie, S. B., Louër, D., Göbel, H. E., Will, G., Gilles, R. & Raftery, T. (1995). *Powder Diffraction*, **10**, 91–95.
- Gebhardt, R., Pechkova, E., Riekkel, C. & Nicolini, C. (2010). *Biophys. J.* **99**, 1262–1267.
- Gehrke, R. (1992). *Rev. Sci. Instrum.* **63**, 455–458.
- Guinier, A. (1963). *X-ray Diffraction in Crystals, Imperfect Crystals and Amorphous Bodies*. New York: Dover.
- Guinier, A. & Fournet, G. (1955). *Small-Angle Scattering of X-rays*. New York: John Wiley and Sons.
- Lazzari, R. (2002). *J. Appl. Cryst.* **35**, 406–421.
- Müller-Buschbaum, P., Gutmann, J. S., Stamm, M., Cubitt, R., Cunis, S., Von Krosigk, G., Gehrke, R. & Petry, W. (2000). *Physica B*, **283**, 53–59.
- Müller-Buschbaum, P., Roth, S. V., Burghammer, M., Diethert, A., Panagiotou, P. & Riekkel, C. (2003). *Europhys. Lett.* **61**, 639–645.
- Nicolini, C. (1997). *Trends Biotechnol.* **15**, 395–401.
- Nicolini, C. & Pechkova, E. (2004). *Expert Rev. Proteom.* **1**, 253–256.
- Nicolini, C. & Pechkova, E. (2006). *J. Cell. Biochem.* **97**, 544–552.
- Pechkova, E., Gebhardt, R., Riekkel, C. & Nicolini, C. (2010a). *Biophys. J.* **99**, 1256–1261.
- Pechkova, E., McSweeney, S. & Nicolini, C. (2010b). *Synchrotron Radiation and Structural Proteomics*, Vol. 3, edited by E. Pechkova & C. Riekkel, pp. 249–275. Singapore: Pan Stanford.
- Pechkova, E. & Nicolini, C. (2002a). *Nanotechnology*, **13**, 460–464.
- Pechkova, E. & Nicolini, C. (2002b). *J. Cell. Biochem.* **85**, 243–251.
- Pechkova, E. & Nicolini, C. (2004a). *Trends Biotechnol.* **22**, 117–122.
- Pechkova, E. & Nicolini, C. (2004b). *J. Cell. Biochem.* **91**, 1010–1020.
- Pechkova, E. & Nicolini, C. (2006). *J. Cell. Biochem.* **97**, 553–560.
- Pechkova, E. & Nicolini, C. (2010). *Anticancer Res.* **30**, 2745–2748.
- Pechkova, E., Roth, S. V., Burghammer, M., Fontani, D., Riekkel, C. & Nicolini, C. (2005). *J. Synchrotron Rad.* **12**, 713–716.
- Pechkova, E., Tripathi, S., Ravelli, R. B., Mcsweeney, S. & Nicolini, C. (2009). *J. Struct. Biol.* **168**, 409–418.
- Pechkova, E., Tropiano, G., Riekkel, C. & Nicolini, C. (2004). *Spectrochim. Acta B*, **59**, 1687–1693.
- Pechkova, E., Zanotti, G. & Nicolini, C. (2003). *Acta Cryst. D* **59**, 2133–2139.
- Rauscher, M., Salditt, T. & Spohn, H. (1995). *Phys. Rev. B*, **52**, 16855–16863.
- Renaud, G., Lazzari, R. & Leroy, F. (2009). *Surf. Sci. Rep.* **64**, 255–380.
- Riekkel, C. (2000). *Rep. Prog. Phys.* **63**, 233–262.
- Roth, V., Burghammer, M., Riekkel, C., Müller-Buschbaum, P., Diethert, A., Panagiotou, P. & Walter, H. (2003). *Appl. Phys. Lett.* **82**, 1935–1937.
- Yoneda, Y. (1963). *Phys. Rev.* **161**, 2010–2013.